ASTM INTERNATIONAL

Journal of Testing and Evaluation

Enrico Lucon[1]

DOI: 10.1520/JTE20180403

Influence of Shear Lip Symmetry on the Fracture Behavior of Charpy Specimens

Journal of Testing and Evaluation

doi:10.1520/JTE20180403 available online at www.astm.org

Enrico Lucon[1]

Influence of Shear Lip Symmetry on the Fracture Behavior of Charpy Specimens

Reference

E. Lucon, "Influence of Shear Lip Symmetry on the Fracture Behavior of Charpy Specimens," *Journal of Testing and Evaluation* https://doi.org/10.1520/JTE20180403

ABSTRACT

An investigation was conducted at the National Institute of Standards and Technology (NIST) on the influence of shear lip symmetry on the fracture behavior (absorbed energy and data scatter) of Charpy specimens at different energy levels, corresponding to NIST low-energy, high-energy, and super-high-energy certified verification specimens. Whenever both shear lips are on the same tested specimen half (symmetrical fracture), absorbed energy tends to be lower than when each specimen half includes one shear lip (asymmetrical fracture). Fracture type does not have a significant effect on impact toughness or variability at low- or high-energy levels, but its influence becomes significant above 200 J. Specifically, super-high-energy specimen lots do not fulfill the NIST requirement (sample size < 5.0) when both fracture types are combined, whereas they may become acceptable if only symmetrical or asymmetrical fractures are considered. This tendency is particularly clear for the 9310 (3-nickel) steel, which is currently under consideration for the reinstatement of super-high-energy specimens in the NIST Standard Reference Materials catalog. The most effective method for preventing the formation of shear lips, and therefore avoiding this type of bimodal behavior, is to side-groove the Charpy specimens for a total thickness reduction of 10 %.

Keywords

asymmetrical fracture, indirect verification Charpy specimens, shear lips, sample size, side-grooving, symmetrical fracture

Manuscript received June 13, 2018; accepted for publication October 4, 2018; published online January 31, 2019.

[1] Applied Chemicals and Materials Division, National Institute of Standards and Technology, Boulder, CO 80305, USA (Corresponding author), e-mail: enrico.lucon@nist.gov, https://orcid.org/0000-0002-3021-4785

Introduction

Charpy impact testing is a low-cost and reliable test method for measuring the impact resistance of materials and is commonly required by construction codes for fracture-critical structures and pressure vessels. In its most common form (notched specimen

struck by a swinging mass, or pendulum), it was introduced between the late 19th century and the early 20th century, through pivotal works by S. B. Russel[1] and G. A. Charpy.[2] It was first standardized by the American Society for Testing and Materials (ASTM) in 1933, when the first version of ASTM E23, *Tentative Method of Impact Testing of Metallic Materials*, was issued as a "tentative" standard test method.[3]

It still took more than 30 years for impact test technology and procedures to reach levels of accuracy and reproducibility such that the method could be broadly applied as an acceptance test for structural materials.[4] Through several decades, the goal of those who have developed and improved the ASTM E23 standard[5] has been (and still is) to standardize and control the variables associated with impact testing, such as specimen size, notch geometry, machine anvils, and striker configuration, and, to a lesser degree, impact velocity, energy losses, and friction.[6]

Charpy testing is often specified as an acceptance test for structural materials. Reliable measurements of impact energy are needed for accurate predictions of the performance of new structures and for predicting when structures are in need of replacement or repair (before catastrophic failure). The impact for replacement and repair scales with the more than $1T (one-trillion dollars) expected to be needed over the next decade to bring the U.S. infrastructure up to safe standards.

The procedure for verifying the performance of impact machines in accordance with both ASTM E23, *Standard Test Methods for Notched Bar Impact Testing of Metallic Materials*,[5] and ISO 148-2, *Metallic Materials – Charpy Pendulum Impact Test – Part 1: Test Method*,[7] consists of a physical part (direct verification) and an experimental part (indirect verification). The direct verification consists in the detailed evaluation of machine dimensions, alignment, and other physical quantities and variables. The indirect verification requires testing sets of Charpy specimens with certified absorbed energy (*KV*) values.

The indirect verification procedure was added to ASTM E23 about 50 years ago, when it was realized that direct verification alone could not explain large and unacceptable differences between machines testing similar specimens.[4] Such differences were traced to interactions between machine components and specimens and could only be resolved by testing very tightly controlled specimens.

During the 1960s, the U.S. Army (Watertown Arsenal, AMMRC, Watertown, MA) started producing and distributing certified Charpy specimens for the indirect verification of impact machines in the United States. The program was taken over by the National Institute of Standards and Technology (NIST) in 1989 when Army personnel helped transfer the three so-called "E23 reference machines" to the NIST Charpy laboratory in Boulder, Colorado. Two of the three original Army machines are still in service after more than 50 years, whereas the third one was replaced in the mid-2000s by a similar one with slightly higher capacity. If the average of the results from an industrial machine agrees with the reference absorbed energy established on the NIST reference machines within the lesser of 1.4 J or 5 %, the machine is indirectly verified in accordance with ASTM E23.

Today, the objective of the Charpy machine verification program at NIST is to evaluate the performance of impact test machines used worldwide to qualify structural steels, by offering customers certified verification specimens that enable certification of their impact machines to a traceable measurement system. The successful indirect verification of machine performance increases the accuracy of impact data, which improves predictions of the reliability of bridges, buildings, railroads, and other infrastructure, as well as the safety of products manufactured from structural steels such as oil and gas pipelines, heavy trucks, mining equipment, power plants, and wind turbines. The existence of this program, in conjunction with the requirements in ASTM E23, has produced a population of industrial impact machines with lower scatter than any other system in the world.[8]

NIST has been offering indirect verification specimens at three absorbed energy levels: low energy ($KV = 13$–20 J), high energy ($KV = 88$–136 J), and super-high energy ($KV = 176$–244 J). Specimens for the first two energy levels are made from AISI 4340 steel, which is subjected to different heat treatments to obtain different levels of hardness and impact toughness.[8] Super-high-energy specimens, historically made from significantly over-aged T200 maraging steel,[8] have been out of stock for the past 10 years, and intensive efforts are underway at NIST to bring them back into the catalog. A different steel (9310), which is currently used by other reference material producers in the world, is also under consideration for producing specimens at the 200 J absorbed energy level.

Formation of Shear Lips in Charpy Specimens: Symmetrical versus Asymmetrical Fracture

The Charpy specimen is a 55-mm-long bar with a 10 by 10 mm cross section and a 2-mm-deep notch with an included angle of 45°. When impacted by a swinging hammer (pendulum) that strikes it on the side opposite the notch while resting against the machine anvils (which are 40 mm apart), the specimen behaves like a single-edge notch bend specimen tested in three-point-bending mode (fig. 1).

During fracture, energy is consumed by initiating and propagating a crack through the specimen but also through plastic deformation, which generates "shear lips." These are narrow ridges or protrusions of material that are caused by specimen bending at the side surfaces, which develop both in height (parallel to the direction of impact) and width (perpendicular to the direction of impact). In the case of a ductile tensile specimen that breaks according to the classical "cup and cone" mode, shear lips appear as narrow, slanting ridges, nominally 45° to the surface, formed along the edge of the fracture. [9] Figure 2 shows an example of shear lips formed in a Charpy test (left) and in a tensile test (right).

In a study published in 1980,[9] the size of the shear lips was found to be correlated to the plane-stress fracture toughness of a commercial high-strength low-allow steel and a cast aluminum alloy, tested in the form of compact

FIG. 1

Schematic of a Charpy impact test.

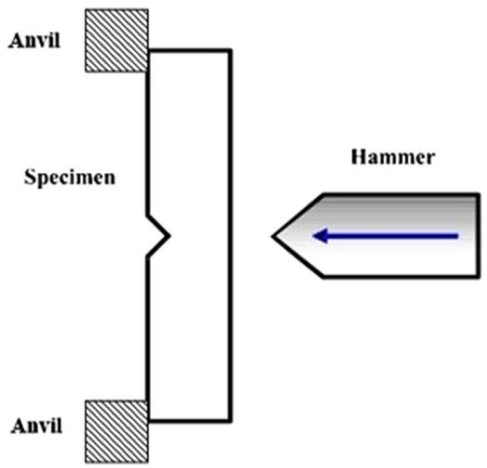

FIG. 2

Illustration of shear lips in Charpy (left) and tensile (right) tests.

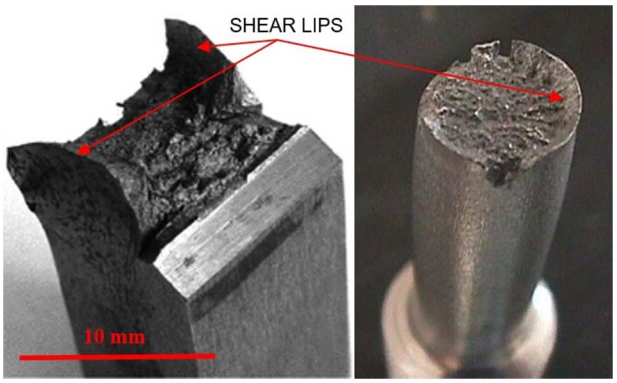

FIG. 3

Role of shear lips in the measurement of lateral expansion (left) and shear fracture appearance (right).

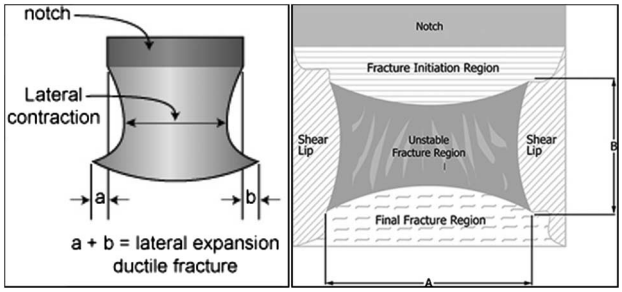

FIG. 4

Comparison between shear lips from a low-energy (left), high-energy (middle), and super-high-energy (right) specimen. All the pictured specimens exhibit symmetrical fracture.

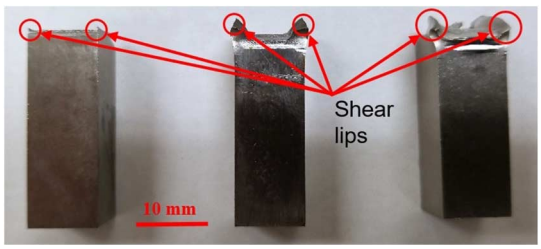

tension specimens. In the same article, the authors stated that shear lips form at the boundary between the elastic zone and the plastic zone that develops ahead of the crack tip. Other sources [10–12] have claimed that shear lips are an indication of a state of plane stress in the material near the lateral surfaces (whereas a state of plane strain generally exists in the middle of the specimen).

In Charpy testing, consideration of shear lips is important when measuring two of the three typical results of an impact test: lateral expansion and shear fracture appearance. Lateral expansion is a measure of ductility that corresponds to the increase in specimen thickness caused by plastic deformation (**fig. 3**, left). Shear fracture appearance is calculated as the ratio between the ductile (shear) portion of the fracture surface and the original (undeformed) cross section of the specimen (**fig. 3**, right).

When assessing lateral expansion, the width of the shear lips protruding beyond the original (undeformed) specimen sides is measured ("a" and "b" in **fig. 3**, left). When calculating shear fracture appearance, the fracture surfaces associated with shear lips are considered as 100 % ductile (**fig. 3**, right).

When a brittle material is tested, or the test temperature is low (corresponding to what is defined as the "lower shelf" of toughness), plastic deformation is very limited, and therefore shear lips are hardly visible. As the toughness or test temperature or both increase, the width and height of the shear lips increase, leading to higher values of lateral expansion, shear fracture appearance, and absorbed energy. Therefore, the magnitude of the shear lips (up to a 3-mm thickness increase) is correlated with the absorbed energy in a Charpy test.

In the case of NIST indirect verification specimens[*], shear lips are tiny at the low-energy level and much more pronounced at both high-energy and super-high-energy levels (**fig. 4**).

Shear lips can be located both on the same broken specimen half (symmetrical fracture), or one on each specimen half (asymmetrical fracture), see **figure 5**. Asymmetrical (A) fractures are typically associated to a

[*]Low-energy and high-energy specimens are tested at −40°C. Super-high-energy specimens are tested at ambient temperature (21°C ± 1°C).

FIG. 5

Examples of asymmetrical (left) and symmetrical (right) fracture for Charpy specimens.

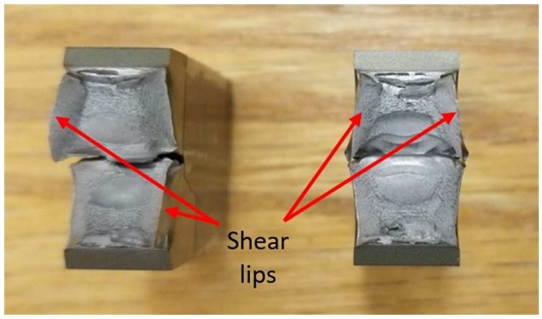

higher Charpy absorbed energy than symmetrical (S) fractures, as shown by a previous NIST study[13] that investigated the effect of fracture mode (S versus A) on the absorbed energies of six high-energy and two super-high-energy lots. Differences ranging from 0 to 5 J at the high-energy level and from 5 to 12 J at the super-high-energy level were reported, which pointed to a maximum increase in energy of about 5 % of the certified value.

The investigation reported here extends this previous study[13] by examining additional specimen lots (including low-energy specimens) and assessing the effect of fracture mode not only on the value of absorbed energy but also on the scatter of NIST verification specimens (standard deviation, coefficient of variation (CV), sample size). Finally, a method to prevent the formation of shear lips (side-grooving) is presented, and its usefulness to guarantee the quality of super-high-energy specimen lots is investigated.

Qualification and Acceptance of NIST Indirect Verification Lots

For an individual lot of Charpy verification specimens to be qualified, NIST tests and examines two groups of 100 specimens each, identified as pilot lot and production lot, respectively. On each lot, dimensional controls, hardness measurements, and 75 impact tests (25 on each reference machine) are performed.[8]

A verification lot is acceptable/qualified if the following hold.

(i) The dimensional measurements are acceptable (NIST tolerances are stricter than specified in ASTM E23);
(ii) hardness is in the expected range (at least 44 HRC [Rockwell-C Hardness] for low energy, 30–33 HRC for high energy, 28–30 HRC for super-high energy);
(iii) the average absorbed energy is in the expected range (typically: 13–20 J for low energy, 88–136 J for high energy, and 176–244 J for super-high energy);
(iv) the sample size, n_{SS}, which is calculated from the results of the three reference machines, does not exceed 5.0.

For a NIST Charpy lot, the sample size corresponds to the minimum number of specimens that a customer has to test for the indirect verification to be statistically valid and is calculated as[8]

$$n_{ss} = \left(\frac{3s_p}{E}\right)^2 \tag{1}$$

where s_p is the pooled standard deviation, defined as the following:

$$s_p = \sqrt{\frac{s_1^2 + s_2^2 + s_3^2}{3}} \tag{2}$$

where s_i = standard deviation of reference machine i, and E is the larger between 1.4 J and 5 % of the mean energy. A larger sample size indicates greater variability of the verification lot.

TABLE 1
Analysis of fracture modes for five low-energy NIST verification lots

		S Fractures		A Fractures		Mean Absorbed Energy, J				Coefficient of Variation, CV				Sample Size			
Lot ID	Number of Tests	Number of Tests	%	Number of Tests	%	All	S	A	Δ_{A-S}	All	S	A	Δ_{A-S}	All	S	A	Δ_{A-S}
LL-85	75	48	64 %	27	36 %	18.63	18.59	18.70	0.6 %	7.7 %	7.6 %	8.0 %	0.4 %	5.28	5.50	5.23	−0.27
LL-87	50	20	40 %	18	36 %	16.72	16.40	16.75	2.1 %	6.9 %	7.6 %	6.6 %	−1.0 %	4.06	4.51	3.81	−0.70
LL-89	74	31	42 %	35	47 %	16.33	16.41	16.28	−0.9 %	6.3 %	5.6 %	7.0 %	1.3 %	1.97	2.14	1.92	−0.23
LL-90	75	30	40 %	38	51 %	14.09	13.88	14.45	4.0 %	6.6 %	6.0 %	5.9 %	−0.1 %	2.28	2.16	1.90	−0.26
LL-168	75	33	44 %	30	40 %	14.70	14.62	14.83	1.4 %	6.8 %	6.5 %	6.7 %	0.2 %	1.44	1.17	1.82	0.65
Mean values			46 %		42 %				1.5 %				0.2 %				−0.16

The certified value of absorbed energy and the expanded uncertainty for the verification lot are calculated from the combined results of the pilot and production lots if no statistical differences are detected between the lots in terms of mean values of standard deviation. Otherwise, only the production lot is used.

Analysis of Test Results from NIST Indirect Verification Lots

Information about the type of fracture (S or A) is not customarily reported when qualification tests are performed at NIST in Boulder, Colorado. However, for a few years between the end of the 1990s and the beginning of the 2000s, the Charpy Program Coordinator noted "S" or "A" next to the absorbed energy recorded in every test. Additionally, the fracture mode for tested specimens from a few recently qualified lots was also recorded. The results are provided in what follows for the three absorbed energy levels.

LOW-ENERGY LOTS

Five low-energy lots from 4340 steel were analyzed (Table 1). As mentioned previously, shear lips are very small at this energy level, and sometimes the type of fracture could not be clearly identified.

Table 1 provides for each lot the following information: number of tests, number and percentage of S and A fractures, mean absorbed energy, CV[†], sample size for all tests, S fractures, and A fractures. Sample sizes are acceptable if not greater than 5.0. Mean values are also provided for some of the parameters (percentages of S and A fractures, differences between S and A in terms of energy, CV, and n_{SS}). Δ_{A-S} indicates the variation (absolute or relative) of a given parameter between A and S fractures.

The results in Table 1 suggest that S and A fractures are almost equally likely to occur at this energy level, while approximately 12 % of fractures cannot be clearly identified. The average absorbed energy is slightly higher when the fracture is asymmetrical (0.22 J, or 1.5 %), which is consistent with previous observations on high- and super-high-energy specimens.[13] The sample size from A fractures is lower than for S fractures.

It can be concluded that the role played by shear lips at the low-energy level is marginal.

HIGH-ENERGY LOTS

Six high-energy lots from 4340 steel have been analyzed (Table 2). One of the lots (HH-96) provided two sets of results (the first failed, the second was re–heat-treated and became acceptable).

At this energy level, the likelihood of either type of fracture appears almost the same. The difference in absorbed energy is more significant, but still generally lower than 5 % (which is the acceptability limit for indirect verification results according to ASTM E23), with A fractures systematically consuming more energy. In terms of variability (both CV and n_{SS}), a minor effect of fracture mode is observed. However, (i) in the case

[†]The coefficient of variation (CV) is given by the ratio between standard deviation and mean value for absorbed energy.

TABLE 2
Analysis of fracture modes for six high-energy NIST verification lots

		S Fractures		A Fractures		Mean Absorbed Energy, J				Coefficient of Variation, CV				Sample Size			
Lot ID	Number of Tests	Number of Tests	%	Number of Tests	%	All	S	A	Δ_{A-S}	All	S	A	Δ_{A-S}	All	S	A	Δ_{A-S}
HH-81	74	45	61 %	29	39 %	83.62	82.78	84.91	2.5 %	1.9 %	1.5 %	1.4 %	−0.1 %	1.32	0.78	0.62	−0.16
HH-85	90	49	54 %	41	46 %	90.61	89.13	92.39	3.6 %	3.3 %	3.0 %	2.6 %	−0.4 %	3.98	3.26	2.42	−0.83
HH-93	75	39	52 %	36	48 %	89.24	87.84	90.76	3.3 %	2.9 %	2.4 %	2.4 %	0.0 %	2.79	1.97	1.52	−0.46
HH-95	118	58	49 %	60	51 %	89.41	89.39	93.20	4.2 %	4.1 %	3.7 %	3.4 %	−0.2 %	4.89	3.93	3.83	−0.11
HH-96	74	40	54 %	34	46 %	111.66	109.05	114.73	5.1 %	4.8 %	3.6 %	4.6 %	1.0 %	7.82	4.24	6.56	2.32
	75	32	43 %	43	57 %	92.64	90.89	93.95	3.3 %	3.0 %	2.8 %	2.4 %	−0.4 %	2.92	1.49	1.77	0.28
HH-151	72	32	44 %	40	56 %	91.50	89.39	93.20	4.2 %	4.1 %	3.7 %	3.4 %	−0.2 %	4.89	3.93	3.83	−0.11
Mean values			51 %		49 %				3.7 %				−0.04 %				0.13

of the only failed lot (the first HH-96), if only S fractures were considered, the lot would be acceptable ($n_{SS} = 4.24$); (ii) when sample sizes from a specific fracture mode are compared to those from all tests, differences start to become significant. Moreover, sample sizes from all tests are always higher than from S or A fractures alone.

In summary, the role played by shear lips becomes significant at the high-energy level but not yet decisive in determining the acceptability of the lot.

SUPER-HIGH-ENERGY LOTS (T200 STEEL)

Eight super-high-energy lots from T200 steel have been analyzed (Table 3). For two of them (SH-22 and SH-24), two pilot lots were available. For the former, both pilot lots failed, whereas for the latter, the second pilot lot was acceptable. In the case of SH-22 (second pilot lot), the fracture type was not indicated for 12 tested specimens (reasons unknown). For lot SH-25, the fracture mode was recorded only for one of the reference machines.

In the super-high-energy range, S fractures become twice as likely as A fractures, in contrast to the low-energy and high-energy ranges, where S and A fractures are almost equally likely. On the absorbed energy front, the relative increase from A fractures (4.6 %) is higher than for high-energy lots (3.7 %) and close to the acceptability limit of ASTM E23 (5 %).

TABLE 3
Analysis of fracture modes for seven super-high-energy NIST verification lots of T200

		S Fractures		A Fractures		Mean Absorbed Energy, J				Coefficient of Variation, CV				Sample Size			
Lot ID	Number of Tests	Number of Tests	%	Number of Tests	%	All	S	A	Δ_{A-S}	All	S	A	Δ_{A-S}	All	S	A	Δ_{A-S}
SH-2	75	42	56 %	33	44 %	220.90	218.15	224.39	2.8 %	4.2 %	4.4 %	3.4 %	−1.0 %	5.98	7.08	3.16	−3.92
SH-16	75	54	72 %	21	28 %	178.00	175.26	185.05	5.4 %	4.0 %	3.4 %	2.5 %	−0.9 %	5.94	4.33	2.28	−2.05
SH-17	75	60	80 %	15	20 %	205.91	204.10	213.16	4.3 %	3.5 %	3.1 %	2.6 %	−0.5 %	3.03	2.26	2.54	0.27
SH-22	50	37	74 %	13	26 %	178.66	173.85	192.35	10.1 %	6.4 %	4.9 %	3.4 %	−1.5 %	14.87	8.74	4.28	−4.47
	65	32	49 %	21	32 %	210.64	206.15	185.05	−10.8 %	4.3 %	3.8 %	2.5 %	−1.3 %	6.45	5.00	2.28	−2.72
SH-24	50	31	62 %	19	38 %	228.23	225.50	232.66	3.1 %	5.3 %	5.5 %	4.4 %	−1.1 %	10.05	10.91	7.03	−3.88
	74	47	64 %	27	36 %	229.22	226.68	233.65	3.0 %	3.4 %	3.0 %	3.0 %	0.0 %	2.91	2.66	2.07	−0.59
SH-25	25	14	56 %	11	44 %	219.78	217.23	223.04	2.6 %	3.4 %	3.3 %	3.0 %	−0.3 %	4.18	4.02	3.28	−0.74
SH-28	68	47	69 %	21	31 %	228.36	226.68	232.13	2.4 %	3.8 %	3.8 %	3.4 %	−0.4 %	5.12	4.88	4.55	−0.33
SH-38	20	15	75 %	5	25 %	169.04	165.74	178.95	7.7 %	5.0 %	2.6 %	5.8 %	3.2 %	8.84	2.39	11.9	9.54
Mean values			67 %		33 %				4.6 %				−0.04 %				−0.68

TABLE 4
Analysis of fracture modes for three experimental super-high-energy lots of 9310

		S Fractures		A Fractures		Mean Absorbed Energy, J				Coefficient of Variation, CV				Sample Size			
Lot ID	Number of Tests	Number of Tests	%	Number of Tests	%	All	S	A	Δ_{A-S}	All	S	A	Δ_{A-S}	All	S	A	Δ_{A-S}
3Ni-1	75	47	64 %	28	38 %	199.34	190.47	214.77	12.0 %	6.5 %	2.7 %	2.7 %	0.1 %	15.49	2.03	2.34	0.31
3Ni-2a	75	56	75 %	19	25 %	190.20	184.30	207.58	11.9 %	6.0 %	2.1 %	3.7 %	1.6 %	12.58	1.06	5.32	4.26
3Ni-2b	98	72	73 %	26	27 %	192.73	186.64	209.60	11.6 %	5.9 %	2.4 %	3.0 %	0.6 %	12.66	2.09	3.12	1.02
Mean values			70 %		30 %				11.8 %				0.8 %				1.86

As far as variability is concerned, specimens breaking asymmetrically have similar coefficients of variation but slightly lower sample sizes (the mean variation in average sample size from A to S is −0.68). Also of importance is the fact that, in most cases, sample sizes are lower when individual fracture types are considered, and therefore mixing of the two fracture modes significantly affects the quality of the verification lot.

SUPER-HIGH-ENERGY LOTS (9310 STEEL)

Three super-high-energy lots from 9310 (3-nickel [Ni]) steel were available for analysis (**Table 4**). All three should be considered experimental pilot lots, heat-treated according to different plans as part of the reinstatement of super-high-energy specimens in the NIST catalogue.

The prevalence of S fractures is even higher than for T200 (70 % versus 30 %), but what is particularly striking is the large difference in terms of absorbed energies (11.8 %), which is more than double the ASTM E23 limit (5 %). Unlike T200, specimens breaking symmetrically exhibit much lower variability (CV lower by 0.8 % and sample size lower by 1.86) than specimens breaking asymmetrically.

It appears that the influence of shear lips and fracture mode is significantly steel-dependent at the super-high-energy level.

SUMMARY OF ANALYSES PERFORMED

The main results of the analyses presented in the preceding sections are summarized in **Table 5**.

Both the number of symmetrical fractures (**fig. 6**) and the energy difference between A and S fractures (**fig. 7**) tend to increase with absorbed energy. At the low-energy level, the importance of fracture mode is negligible in terms of both energy and variability (sample size). The role of shear lips becomes more significant at the high-energy level, although it does not appear crucial in determining the acceptability of a lot. For super-high-energy specimens, the influence of fracture mode can be hardly neglected—particularly for the 9310 steel, it is difficult to obtain an acceptable lot when symmetrical and asymmetrical fractures are combined. The relationship between the sample size from all tests and from a specific fracture mode is illustrated in **figure 8**. It is interesting to note that, overall, the relative comparison between the sample size of asymmetrical and symmetrical fractures varies across the range of lots examined.

TABLE 5
Summary of fracture mode analyses performed on NIST Charpy verification lots (mean values)

		Percent of Tests		Diff. in Mean *KV* (A versus S)		Sample Size		
Energy Level	Steel	S	A	J	%	All	S	A
Low	4340	46 %	42 %	0.22	1.5 %	3.01	3.10	2.94
High	4340	51 %	49 %	3.52	3.7 %	4.09	2.80	2.94
Super-High	T200[a]	67 %	33 %	9.13	4.6 %	6.77	5.25	4.57
	9310	70 %	30 %	23.51	11.8 %	13.57	1.73	3.59

Note: [a] Excluding the second pilot lot of lot SH-22.

FIG. 6

Percentages of S and A fractures as a function of mean absorbed energy. NOTE: fitting lines are just a guide for the eye.

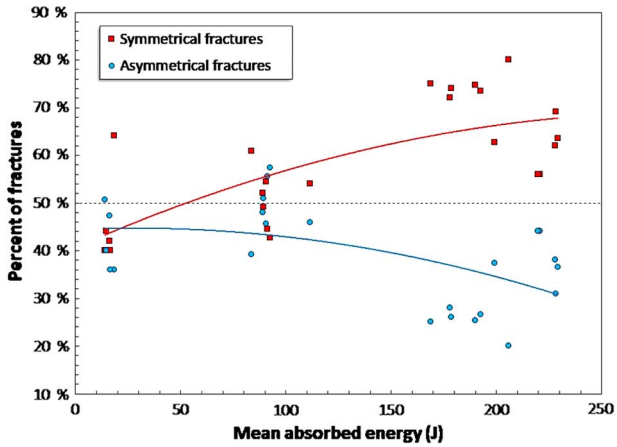

FIG. 7

Absorbed energy difference between A and S fracture. The 9310 steel yields the largest differences. NOTE: the fitting line is just a guide for the eye.

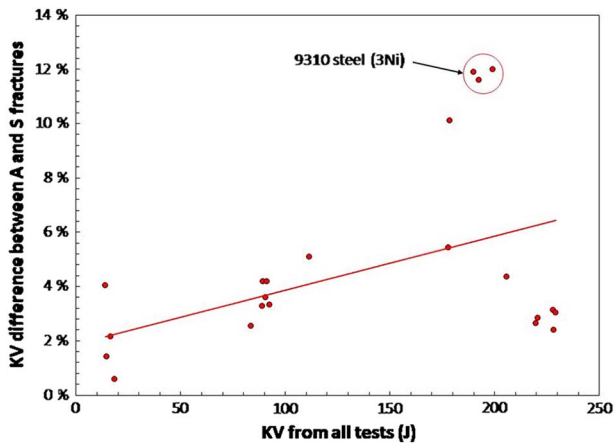

FIG. 8

Sample sizes calculated for all tests and for specific fracture types. NOTE: fitting lines are just a guide for the eye.

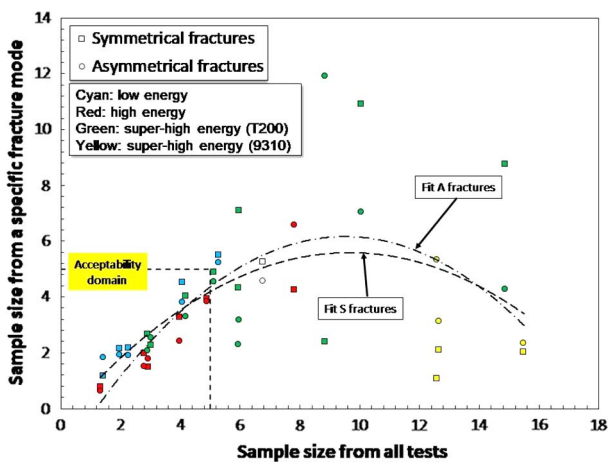

From the comparison between results of T200 and 9310 at the super-high-energy level, it is quite evident that the latter steel exhibited a much more distinct bimodal behavior, with symmetrical and asymmetrical specimens behaving almost like two different materials. Hence, consideration of the 9310 steel for the production of super-high-energy verification specimens must certainly account for the influence of shear lip symmetry.

Influence of Specimen Squareness and Ligament Size on Fracture Symmetry

One of the geometrical factors that might affect the likelihood of a Charpy specimen fracturing in an asymmetrical fashion is the squareness/perpendicularity[‡] (or lack thereof) between specimen and machine (supports and anvils) or specimen and striker. Specifically, if the angles between specimen sides or between specimen and machine parts are not exactly 90°, the specimen might tilt slightly at the moment of impact, and this could cause shear lips to split between specimen halves.

The issue was already examined (or at least mentioned) in the previous NIST study,[13] but no correlation was found between squareness and energy or fracture mode.

This aspect was also considered in the present investigation, as well as the possible influence of a lack of perpendicularity between notch root and specimen edges[§]. A set of twenty T200 super-high-energy specimens (lot ID: SH-38) was subjected to the following pre-test measurements:

(i) Squareness between specimen sides and upper specimen surface (anvil side) and between specimen sides and lower specimen surface (striker side). These measurements were performed by means of a special device that was equipped with a dial gage (**fig. 9**). As shown on the right side of the figure, these linear measurements can easily be correlated to deviations from perpendicularity (90° angles) and thus checked against the requirements and tolerances from ASTM E23 (90° ± 0.17°) and from NIST (90° ± 0.15°) for verification specimens.

(ii) Ligament size (i.e., distance between the tip of the notch and the lower side of the specimen) on the two lateral surfaces of the specimen by means of an optical comparator (profile projector) (**fig. 10**).

Table 6 presents the deviations from perpendicularity of adjacent specimen sides measured by means of the setup pictured in **figure 9**. Only one of the recorded deviations exceeded both the ASTM E23 and the NIST tolerances on perpendicularity (specimen 145, striker side).

Measurements of ligament size on the specimen side surfaces are collected in **Table 7** along with their absolute differences. None of the individual measurements exceed the limits prescribed by ASTM E23 (8 mm ± 0.025 mm), which coincide with the NIST requirements for verification specimens.

In order to combine the results of the measurements performed, we defined an "Out-of-Tolerance" (OOT) index for each specimen, which can be best explained by referring to **Table 8**. If a specimen was found to provide one of the five extreme measurements (i.e., largest deviations from the nominal value) in **Tables 6** and **7**, it was given an asterisk (*) in the corresponding column of **Table 8**. The total number of asterisks corresponds to the OOT index for each specimen, between 0 (best) and 3 (worst). The higher is the OOT index, the more "imperfect" is the specimen.

The calculated OOT indexes were correlated with the energy absorbed by each specimen in **figure 11**, where the type of fracture is indicated by a different color (blue for symmetrical, red for asymmetrical). The figure shows absorbed energy increasing with OOT for asymmetrical fractures and decreasing for symmetrical fractures, but

[‡]ASTM E23 requires that the angle between adjacent specimen sides be 90° ± 0.17°. NIST specifications for verification specimens prescribe a slightly tighter tolerance of ± 9' (± 0.15°).

[§]ASTM E23 requires that the angle between notch length and specimen edges be 90° ± 2°. NIST specifications for verification specimens prescribe a much tighter tolerance of ± 9' (± 0.15°).

FIG. 9 Special device used for squareness measurements (left) and illustration of the measurements performed (right).

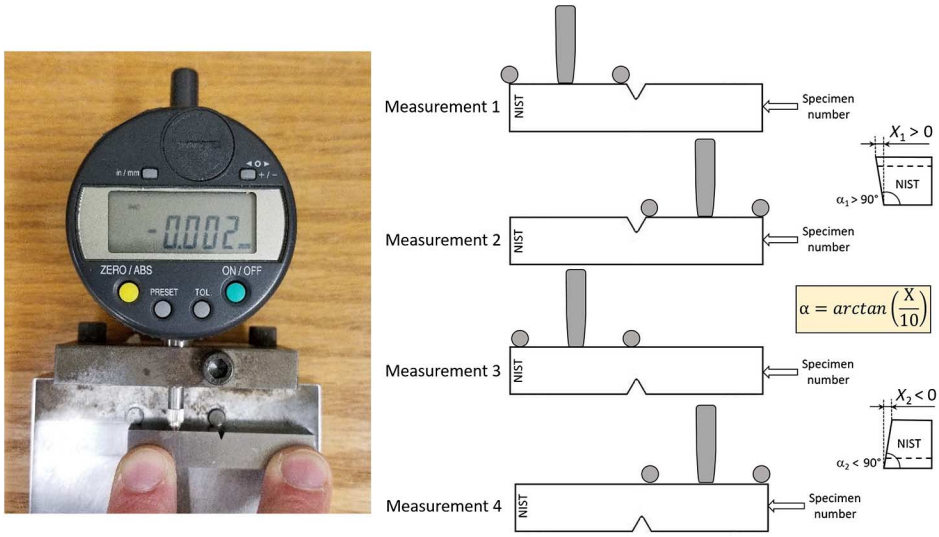

FIG. 10

Illustration of ligament size measurements performed by means of an optical comparator.

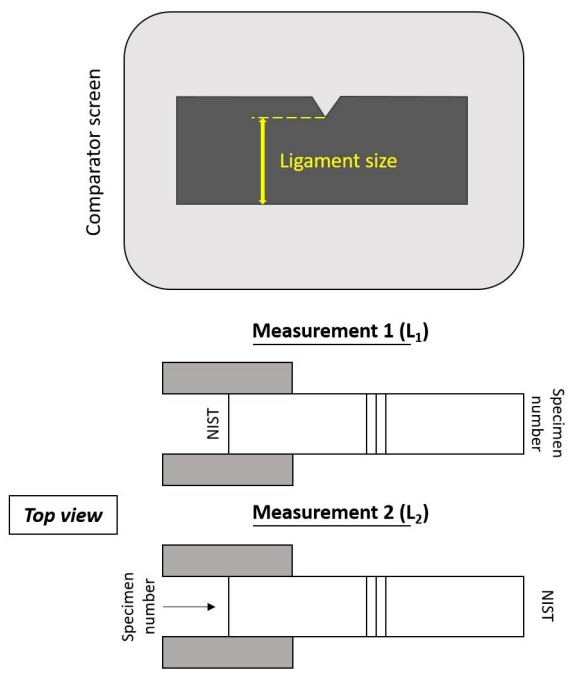

both calculated slopes are not statistically different from 1 at the 95 % confidence level, as demonstrated by a simple ANOVA analysis. Furthermore, no obvious correlation between shear lip symmetry and OOT index can be detected from figure 11. For example, most of the specimens corresponding to the highest high OOT indexes (2 or 3) exhibited symmetrical fracture.

TABLE 6

Deviations from squareness between specimen sides measured on T200 specimens (see also **fig. 9**)

	Deviation from Squareness Anvil Side [X_1]				Deviation from Squareness Striker Side [X_2]			
Specimen ID	M_1, mm	M_2, mm	Average $M_1-M_2=X_1$	α_1, °	M_3, mm	M_4, mm	Average $M_3-M_4=X_2$	α_2, °
1430	0	−0.001	−0.0005	89.997	0.002	0.002	0.002	90.011
986	−0.002	−0.01	−0.006	89.966	0.016	0.017	0.0165	90.095
56	−0.025	−0.024	−0.0245	89.860	−0.008	−0.009	−0.0085	89.951
3	0.005	0.005	0.005	90.029	−0.001	−0.003	−0.002	89.989
145	0.033	0.017	0.025	90.143	0.081	0.078	0.0795	90.455
576	−0.003	−0.005	−0.004	89.977	−0.005	−0.005	−0.005	89.971
1449	−0.019	−0.003	−0.011	89.937	−0.006	−0.011	−0.0085	89.951
564	0.001	0	0.0005	90.003	−0.003	−0.008	−0.0055	89.968
82	−0.005	−0.002	−0.0035	89.980	−0.006	−0.003	−0.0045	89.974
811	−0.003	−0.007	−0.005	89.971	0.018	−0.017	0.0005	90.003
755	0	−0.001	−0.0005	89.997	−0.004	−0.006	−0.005	89.971
1024	0	−0.002	−0.001	89.994	0.007	−0.011	−0.002	89.989
580	0.024	0.025	0.0245	90.140	0	0.001	0.0005	90.003
323	0.006	0.009	0.0075	90.043	−0.005	−0.002	−0.0035	89.980
758	0	0	0	90.000	0.005	0.006	0.0055	90.032
696	0.002	0.001	0.0015	90.009	0.005	0.005	0.005	90.029
356	0.014	0.014	0.014	90.080	0.004	0.003	0.0035	90.020
671	0.007	0.001	0.004	90.023	0.002	−0.008	−0.003	89.983
912	0.012	0.01	0.011	90.063	0.003	0.001	0.002	90.011
1444	−0.008	0.001	−0.0035	89.980	0.007	0.001	0.004	90.023

TABLE 7

Measurements of ligament size on the specimen side surfaces (see also **fig. 10**) and relevant differences

Specimen ID	b_1, mm	b_2, mm	$\lvert\Delta\rvert$, mm
1430	7.990	7.991	0.001
986	7.987	7.999	0.012 [a]
56	7.994	7.994	0.000
3	7.995	7.994	0.001
145	7.998	7.995	0.003
576	8.000	8.005	0.005
1449	7.998	7.990	0.008
564	8.003	7.999	0.004
82	7.989	8.000	0.011
811	8.001	7.998	0.003
755	7.994	7.992	0.002
1024	8.002	8.003	0.001
580	7.999	8.002	0.003
323	7.997	7.999	0.002
758	8.004	8.007	0.003
696	8.002	8.008	0.006
356	8.007	8.002	0.005
671	8.002	7.998	0.004
912	7.998	7.995	0.003
1444	7.993	7.995	0.002

Note: [a] The six largest differences are in red background.

TABLE 8
Out-of-tolerance indexes for each of the specimens tested

Specimen ID	Squareness		Ligament Size	OOT Index [a]	*KV*, J	Fracture Mode
	Anvil	Striker				
1430				0	171.04	S
986		*	*	2	166.23	S
56	*	*		2	163.17	S
3				0	170.67	S
145	*	*		2	162.51	S
576			*	1	162.14	S
1449	*	*	*	3	181.41	A
564		*		1	156.92	S
82			*	1	162.42	S
811				0	169.56	S
755				0	167.99	S
1024				0	167.16	S
580	*			1	166.78	A
323				0	166.60	S
758		*		1	167.71	S
696			*	1	189.67	A
356	*			1	187.23	A
671				0	160.65	S
912	*			1	169.65	A
1444				0	171.32	S

Note: OOT = Out-of-Tolerance;[a] Color Codes: GREEN – 0; BLUE – 1; RED – 2 or 3).

Side-Grooving Charpy Specimens to Prevent the Formation of Shear Lips

In elastic-plastic fracture mechanics testing, specimen side-grooving is used with two primary objectives:

(i) promoting more uniform crack growth during both fatigue precracking and testing by removing the layers adjacent to the specimen side surfaces, and therefore counteracting the effect of crack tunneling[**,14,15];
(ii) enhancing stress triaxiality throughout a larger part of the crack front by avoiding direct boundaries between the crack tip and the lateral surfaces of the specimen. The level of crack-tip constraint increases by reducing the volume of material subject to a state of plane stress. The resulting effect on fracture toughness is equivalent to an increase in specimen thickness.

Side-grooving of Charpy specimens is customarily applied when using fatigue precracked Charpy-type samples for measuring ductile crack resistance,[16–19] but almost never in conventional impact testing. In this investigation, it was used for preventing the formation of shear lips caused by plastic deformation in super-high-energy specimens.

TESTS ON SIDE-GROOVED T200 SPECIMENS

Fifty-six super-high-energy specimens from T200 steel (original lot ID: SH-38) were side-grooved with the following geometrical parameters: angle—45°; root radius—0.25 mm; depth—0.5 mm per side (total thickness reduction, 1 mm = 10 %).

[**] Tunneling is observed when crack growth occurs mostly in the mid-thickness portion of the crack front, whereas it is significantly retarded in the proximity of the specimen's lateral surfaces.

FIG. 11

Correlation between OOT index, absorbed energy, and fracture type for T200 secimens.

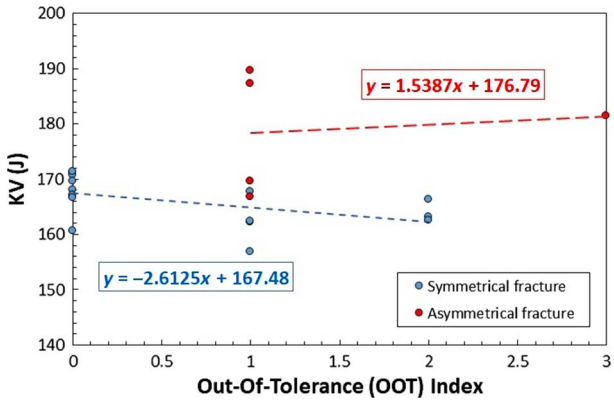

The side-grooved specimens were tested at room temperature (21°C ± 1°C) on the three NIST reference machines (18 or 19 tests per machine). The results are summarized in Table 9, which compares them with the data from the original qualification tests performed on the SH-38 pilot lot in 2009.

The effect of side grooving is extremely significant and clearly beneficial in terms of variability. Namely, standard deviation is almost cut in half (from 8.19 to 4.21 J) and the coefficient of variation drops from 4.7 % to 3.4 %. The most significant improvement is, however, the decrease of sample size from 7.3 to 2.0.

Predictably, absorbed energy drops significantly (by about 30 %). Considering that the cross-section reduction caused by side-grooving is only 10 %, we can attribute the remaining 20 % drop in absorbed energy to the increase in crack-tip constraint.

TESTS ON SIDE-GROOVED 9310 SPECIMENS

With 9310 Charpy specimens, two side-groove depths were investigated, corresponding to 5 % (side-groove depth = 0.25 mm per side, 0.5-mm total thickness reduction) and 10 % (0.5 mm per side, as noted previously for T200). Angle and root radius were the same for all specimens.

For each side-groove depth, we tested 45 Charpy specimens (15 on each reference machine) at room temperature. The material (9310 steel) is directly comparable, in terms of heat treatment, with the 3Ni-2b lot in Table 4. The comparison between plane-sided, 5 % side-grooved, and 10 % side-grooved test results is presented in Table 10.

TABLE 9

Comparison between results from plain-sided (i.e., non-side-grooved) and 10 % side-grooved T200 specimens (lot SH-38)

Specimen Type	Number of Tests	Mean *KV*, J	Standard Dev., J	Range [a], J	CV	Sample Size
Plain-sided	74	174.09	8.19	37.02	4.7 %	7.294
10 % s-g	56	123.57	4.21	17.23	3.4 %	2.025

Note: [a] Range is the difference between highest and lowest absorbed energy.

TABLE 10

Comparison between results from plain-sided, 5 % side-grooved, and 10 % side-grooved 9310 specimens

Specimen Type	Number of Tests	Mean *KV*, J	Standard Dev., J	Range, J	CV	Sample Size
Plain-sided (3Ni-2b)	98	192.73	11.33	42.31	5.9 %	12.657
5 % s-g	45	197.86	7.77	34.65	3.9 %	5.768
10 % s-g	45	171.84	7.38	29.31	4.3 %	2.388

Side-grooving has similar effects on the variability of 9310 as for T200: decrease of standard deviation, range of absorbed energy, coefficient of variation, and sample size. However, it is interesting (and somewhat unexpected) to note that 5 % side grooving, despite a lower value of CV, does not decrease the mean absorbed energy and yields a slightly unacceptable sample size. Conversely, results from 10 % side-grooved specimens are clearly acceptable; the drop in absorbed energy is just 10.8 %, i.e., almost the same as the decrease in specimen cross section (10 %). The additional contribution of crack-tip constraint appears therefore almost negligible.

These results and the comparison with Table 9 confirm the significantly different behaviors of the two materials currently under consideration at NIST for super-high-energy specimens: T200 (18Ni) and 9310 (3Ni).

FINAL REMARKS ON SIDE GROOVING AND A POSSIBLE ALTERNATIVE APPROACH

The results presented previously indicate that side-grooving super-high-energy specimens is very effective in controlling the variability of the lots, both for T200 and 9310, by preventing the formation of shear lips. A 10 % side-groove depth (0.5 mm per side) appears more effective than 5 % (0.25 mm per side), at least in the case of 9310. Shear lips are not observed with either type of side-grooves.

However, the main drawback is the reduction in absorbed energy that is caused by the combined effects of the reduction in below-notch cross section and the increase of crack-tip constraint (which appears more significant for T200). Because the typical absorbed energy range for super-high-energy specimens according to ASTM E23 is 176–244 J, it will be necessary to adjust the heat treatments so that the energy level for the plane-sided specimens would be at least 250 J for T200 and 220 J for 9310 (based on the *KV* drops recorded in Tables 9 and 10 for 10 % s-g specimens).

Another downside is the additional cost of side-grooving. However, considering the number of specimens in a typical verification lot (between 1,600 and 2,000), the additional cost should be kept to a reasonable level and should therefore only marginally affect the retail price of the specimens.

An interesting alternative to side-grooving would be to only consider one type of fracture (symmetrical or asymmetrical) for verifying a Charpy machine at the super-high-energy level.

For example, under the assumption that the values for 9310 in Table 5 are of general applicability, only two symmetrical specimen test results would be needed for a statistically valid machine verification (sample size = 1.73). Because the relative percentage of S fractures was found to be 70 %, the statistical likelihood of having at least two symmetrical fractures in a set of five super-high-energy 9310 specimens is 96.9 % (see Table 11 for details).

That said, our intention is to adopt side-grooving as the primary methodology moving forward.

Future Research

The activities described in this article are part of a work in progress. We are also hoping to identify new materials or improved heat treatments, or both, that could enable us to produce acceptable super-high-energy verification lots without resorting to side-grooving or analyzing just one type of fracture.

TABLE 11

Statistical probabilities of having between 0 and 5 symmetrical or asymmetrical fractures in a set of 5 NIST super-high-energy verification specimens of 9310 steel, based on an overall population of 70 % S and 30 % A

Type of Fracture	Number of Occurrences (Out of Five Tests)					
A	0	1	2	3	4	5
S	5	4	3	2	1	0
Probability	16.8 %	36.0 %	30.9 %	13.2 %	2.8 %	0.2 %
Probability of having at least two S fractures in a set of five verification specimens						96.9 %
Probability of having less than two S fractures in a set of five verification specimens						3.1 %

As far as the study of shear lip symmetry in Charpy testing of very ductile materials is concerned, the next planned steps of the investigation are the following:

(1) Microstructural investigations: differences in mechanical behavior (symmetrical versus asymmetrical fracture) within the same lot can be tied back to differences in heat treatment, which can undoubtedly influence the microstructure. Determining this change in microstructure can provide extended insight into strengthening and failure mechanisms. The planned work on microstructural analysis includes determining changes in grain size and phase distributions, such as carbide precipitates, as even small variations in these factors have been found to have pronounced effects on mechanical performance. Understanding these factors can help determine a procedure for producing uniform and consistent Charpy verification specimens.
(2) Strain analyses: the presence of shear lips occupying a significant portion of the fracture surface is indicative of a mixed-mode, three-dimensional state of stress and strain at fracture. ASTM sets standards for specimen geometry in an attempt to ensure fully plane-strain conditions at fracture; however, it is clear from the fracture surfaces that such conditions are insufficient for super-high-energy Charpy specimens. Additionally, the bimodal nature of the symmetric/asymmetric fracture even for identically prepared specimens hints at a complicated stress/strain state beyond distinguishing between plane-stress and plane-strain. A true understanding of the stress/strain state in these specimens is necessary. Although no technique exists to measure the strain at a rate fast enough to measure the strain evolution throughout an impact test, synchrotron X-ray or neutron diffraction-based techniques are suitable for measuring one or two components of strain in loaded Charpy specimens. Emerging techniques based on neutron Bragg edge transmission[20] may be suitable for a complete determination of the three-dimensional state of strain.

Conclusions

An investigation on the influence of shear lip symmetry on the fracture of Charpy specimens was conducted at NIST in the framework of activities aimed at reinstating super-high-energy verification specimens in the NIST Standard Reference Materials catalog.

The effect of symmetrical (both shear lips on the same tested specimen half) or asymmetrical (one shear lip per specimen half) fracture on the absorbed energy (*KV*) level and variability (standard deviation, coefficient of variation, and sample size) of NIST Charpy verification specimen lots was examined for three energy levels (low: around 17 J; high: around 100 J; super high: around 200 J), by examining old qualification tests and conducting new tests. The most significant conclusions of this study to date are the following.

- Shear lips, caused by plastic deformation during three-point bending of the Charpy specimen, can be detected even at low-energy levels, even though the type of fracture (S or A) cannot always be identified.
- Consistent with previously published studies, asymmetrically broken specimens tend to absorb more energy. The difference between A and S tends to increase with increasing *KV* and approaches or exceeds the ASTM E23 indirect verification requirement (5 % of mean *KV*) at the super-high-energy level.
- The likelihood of S fracture also tends to increase with absorbed energy level, ranging from about 50 % for low- and high-energy specimens to about 70 % for super-high-energy specimens. We observed a slightly higher proportion of S fractures for the 9310 (3Ni) steel than for the T200 (18Ni) steel.
- In terms of result variability, shear lip symmetry has a negligible influence for low-energy specimens. At the high-energy level, considering only one type of fracture lowers the sample size but does not seem to affect the acceptability (sample size $n_{SS} \leq 5.0$) of the lot. For super-high-energy specimens, and particularly for the 9310 steel, shear lip symmetry is so influential that this behavior can be defined as bimodal. Even if the overall behavior of the lot is unacceptable ($n_{SS} > 5.0$), consideration of just one type of fracture would often yield an acceptable material.
- The possible effect of deviations from the prescribed squareness and perpendicularity of the specimens was investigated on a set of T200 specimens. Our results do not show any clear evidence of such an effect.

- One of the most effective ways to prevent the formation of shear lips is side-grooving the Charpy specimens. For super-high-energy specimens, a total thickness reduction of 10 % (depth = 0.5 mm per side) was found extremely effective for significantly lowering the sample size on both T200 and 9310. For the latter steel, 5 % side-grooving was not found equally effective.
- The decrease in absorbed energy caused by side-grooving, as a result of below-notch reduction of cross section and enhanced crack-tip constraint, appears to be more significant for T200 (~30 %) than for 9310 (~11 %). In order to maintain the mean absorbed energy at the level prescribed by ASTM E23 (between 176 and 244 J), it will be necessary to modify the heat treatment of the steels to achieve a higher energy level for the plane-sided specimens (between 220 and 250 J).

ACKNOWLEDGMENTS

My gratitude goes to Ray Santoyo for his assistance in retrieving and analyzing old qualification test results and to May Martin and Matt Connolly for their suggestions concerning future activities (microstructural investigations and strain analyses, respectively).

References

1. S. B. Russell, "Experiments with a New Machine for Testing Materials by Impact," *Transactions of the American Society of Civil Engineers* 39, no. 826 (June 1898): 237–263.
2. G. A. Charpy, "Note sur l'essai des métaux à la flexion par choc de barreaux entaillés," in *Mémoire et compte-rendus de la Société des ingénieurs civils de France* (Paris, 1901): 848–877.
3. *Tentative Method of Impact Testing of Metallic Materials*, ASTM E23-33T (West Conshohocken, PA: ASTM International, 1933).
4. D. E. Driscoll, "Reproducibility of Charpy Impact Test," in *Symposium on Impact Testing, ASTM STP176*, ed. F. Tatnall, (West Conshohocken, PA: ASTM International, 1955), 70–75. https://doi.org/10.1520/STP47578S
5. *Standard Test Methods for Notched Bar Impact Testing of Metallic Materials* (Superseded), ASTM E23-16b (West Conshohocken, PA: ASTM International, 2016). https://doi.org/10.1520/E0023-18
6. N. Fahey, "The Charpy Impact Test–Its Accuracy and Factors Affecting Test Results," in *Impact Testing of Metals*, ed. D. Driscoll (West Conshohocken, PA: ASTM International, 1961), 76–92. http://doi.org/10.1520/STP466-EB
7. *Metallic Materials – Charpy Pendulum Impact Test – Part 1: Test Method*, ISO 148-1:2016 (Geneva, Switzerland: International Standardization Organization, 2016). www.iso.org.
8. C. N. McCowan, T. A. Siewert, and D. P. Vigliotti, "The NIST Charpy V-Notch Verification Program: Overview and Operating Procedures," in *Charpy Verification Program: Reports Covering 1989-2002, NIST Technical Note 1500-9*, (Gaithersburg, MD: National Institute of Standards and Technology, 2003): 3–42.
9. M. O. Lai and W. G. Ferguson, "Relationship between the Shear Lip Size and the Fracture Toughness," *Materials Science and Engineering* 45, no. 2 (September 1980): 183–188, https://doi.org/10.1016/0025-5416(80)90224-4
10. K. E. McKinney, W. L. Bradley, and P. C. Gerhardt Jr., "An Evaluation of the Toughness of Ductile Iron vs. Cast Steel Using Modified Charpy Test Specimens," *Transactions of the American Foundrymen's Society* 92 (1984): 239–250.
11. S. W. Becker and M. N. Srinivasan, "Fatigue and Fracture Toughness of Cast Irons," in *ASM Handbook, Vol 19: Fatigue and Fracture*, ed. S. R. Lampman (Materials Park, OH: ASM International, 1996): 665–679.
12. R. A. Martínez, R. E. Boeri, and J. A. Sikora, "Impact and Fracture Properties of ADI, Compared with SAE 4140 Steel," *Transactions of the American Foundrymen's Society* 106, no. 4 (1998): 27–30.
13. C. N. McCowan and D. P. Vigliotti, "The Influence of Shear Lip Symmetry on the Absorbed Energy of Charpy Impact Specimens," in *Charpy Verification Program: Reports Covering 1989-2002, NIST Technical Note 1500-9*, (Gaithersburg, MD: National Institute of Standards and Technology, 2003): 287–293.
14. J. Zuo, X. Deng, M. A. Sutton, and C.-S. Cheng, "Crack Tunneling: Effect of Stress Constraint," in *ASME 2004 International Mechanical Engineering Congress and Exposition* (New York: American Society of Mechanical Engineers, 2004): 393–400.
15. W. Lan, X. Deng, and M. A. Sutton, "Investigation of Crack Tunneling in Ductile Materials," *Engineering Fracture Mechanics* 77, no. 14 (September 2010): 2800–2812, https://doi.org/10.1016/j.engfracmech.2010.06.010
16. E. Smith and B. M. Patchett, "Effects of Notch Acuity and Side Grooving on Fracture Toughness," *Welding Research Supplement* (July 1975): 226-s–233-s.
17. W. L. Server, R. A. Wullaert, and R. O. Ritchie, "On the Use of Side-Grooves in Estimating J_{Ic} Fracture Toughness with Charpy-Size Specimens," *Journal of Engineering Materials and Technology* 102, no. 2 (April 1980): 192–199, https://doi.org/10.1115/1.3224796
18. E. Morland, "Fracture Toughness in the Transition Regime for A533B-1 Steel: The Effect of Specimen Sidegrooving," in *Fracture Mechanics: Twenty-First Symposium*, *ASTM STP1074*, ed. J. P. Gudas, J. A. Joyce, and E. M. Hackett (West Conshohocken, PA: ASTM International, 1990): 215–237. https://doi.org/10.1520/STP18997S

19. X. P. Zhang and Y. W. Shi, "Constraint of Side-Groove and Its Influence on Fracture Toughness Parameter in Charpy-Size Specimens," *Engineering Fracture Mechanics* 43, no. 5 (November 1992): 863–867, https://doi.org/10.1016/0013-7944(92)90016-8
20. M. J. Connolly, P. E. Bradley, A. J. Slifka, and E. S. Drexler, "In situ Neutron Transmission Bragg Edge Measurements of Strain Fields near Fatigue Cracks Grown in Air and in Hydrogen," in *International Hydrogen Conference (IHC 2016): Materials Performance in Hydrogen Environments*, ed. B. P. Somerday and P. Sofronis (New York: American Society of Mechanical Engineers, 2017).